Letters

Integrated Driving/Charging/Discharging Battery-Powered Four-Phase Switched Reluctance Motor Drive With Two Current Sensors

Hung-Chi Chen, *Senior Member, IEEE*, Wei-An Wang, and Bo-Wei Huang

***Abstract*—In this letter, the motor drive for four-phase switched reluctance motor (SRM) with only two current sensors is proposed. The asymmetric half-bridge circuit is used, but each of the two winding currents is sensed by one current sensor, which makes the proposed SRM drive able to provide additional charging/discharging functions without adding any extra circuit component, extra current sensor, and selector. The integrated drive is implemented and demonstrated by the provided results.**

***Index Terms*—Battery charger, current sensor, switched reluctance motor drives.**

I. Introduction

DUE to no winding and permanent magnet in the rotor of a switched reluctance motor (SRM), it possesses high efficiency with wide speed range and potential applications in electrical vehicle (EV) and hybrid EV [1]–[6]. For battery-powered SRM drive, a front-end dc/dc converter is often connected between the battery and the SRM drive to boost the battery voltage to dc-link voltage [5]–[8].

However, the use of a separate charger limits the portability of such a system, as the system has to be constantly accompanied by a separate battery charging device if continuous operation is required. Because of negligible mutual inductance between the SRM windings and no permanent magnet in SRM rotor, the SRM windings can be used to provide charging function [2]–[9] when SRM is at a standstill.

To integrate the driving/charging function, some special SRM winding arrangements are required in the literature, but their cost is higher than the common winding arrangements. In [4], the center-tapped SRM windings are required for integrated charging function. In [9], the use of coupled windings allows the motor and power converter to function as a battery charger where the coupled windings are employed as a high-frequency isolation transformer.

Manuscript received August 14, 2018; revised August 31, 2018 and October 9, 2018; accepted November 5, 2018. Date of publication November 9, 2018; date of current version April 20, 2019. This work was supported by the Ministry of Science and Technology (MOST) of Taiwan under Grant MOST-107-2622-E-009-008-CC3. *(Corresponding author: Hung-Chi Chen.)*

H.-C. Chen is with the Department of Electrical and Computer Engineering, National Chiao Tung University, Hsinchu 30010, Taiwan, R.O.C. (e-mail:

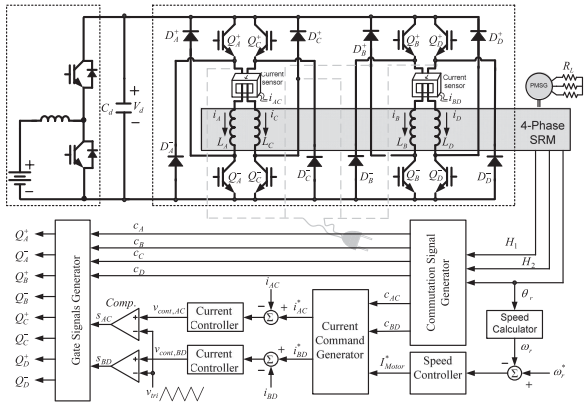

Fig. 1. Integrated four-phase SRM drive and its motor driving control.

The common SRM winding is often used to integrate the charging operation. In [2], [7], and [8], the connection of ac plug makes the SRM winding and the diodes acting as the bridge rectifier, and the front-end converter handles the charging function.

In [3], [5], and [6], either the ac plug voltages or the generator voltages are connected to the diode rectifier to generate the dc-link voltage of the SRM drive. And the energy is transferred to the battery by the front-end converter. However, the above methods in [2]–[9] cannot provide discharging operation.

Recently, some attentions are put on the ability to transfer energy from the battery to grid. In [10], integrated driving/charging/discharging functions are provided, but many selectors and extra inductors need to be added to the topology.

In this letter, the battery-powered four-phase SRM drive integrated driving/charging/discharging functions with only two current sensors is proposed. The common bidirectional dc/dc converter is connected between the battery and the proposed SRM drive topology to regulate the dc-link voltage, as plotted in Fig. 1. The same SRM drive topology can be directly used for charging/discharging operation without adding any extra circuit component, extra current sensor, and selector. Finally, the

proposed integrated drive is implemented and demonstrated by the provided results.

II. Integrated SRM Drive

Fig. 1 shows the proposed integrated four-phase SRM drive. Four-leg asymmetrical half-bridge converter is used to yield the four winding currents $i_A \sim i_D$, where each leg is composed of two switches and two diodes. The frond-end bidirectional dc/dc converter with battery input is used to provide a regulated dc-link voltage $V_{\rm dc}$.

According to the winding distribution in four-phase SRM, the inductance functions $L_C(\theta_r)$ and $L_D(\theta_r)$ can be expressed in terms of the phase-shifted function of $L_A(\theta_r)$ and $L_B(\theta_r)$, respectively, where θ_r is the rotor position

$$L_C(\theta_r) = L_A(\theta_r - \pi) \tag{1}$$

$$L_D(\theta_r) = L_B(\theta_r - \pi). \tag{2}$$

As plotted in Fig. 1, one physical current sensor is used to sense the currents i_A and i_C simultaneously, and the other current sensor senses the currents i_B and i_D at the same time. Thus, the sensed currents i_{AC} and i_{BD} can be expressed as

$$i_{AC} = i_A + i_C \tag{3}$$

$$i_{BD} = i_B + i_D. \tag{4}$$

A. Motor Driving Control

Two Hall-sensor signals $H_1 \sim H_2$ and the position signal θ_r are used to provide the commutation signals $c_A \sim c_D$ to the gate signal generator. The commutation signals c_{AC} and c_{BD} are generated for the current command generator. The position signal θ_r is also used to calculate the motor speed ω_r. The illustrated waveforms are plotted in Fig. 2. The current command amplitude $I^*_{\rm Motor}$ is generated by the speed controller.

In addition, the current commands i^*_{AC} and i^*_{BD} are generated by the current command generator

$$i^*_{AC} = I^*_{\rm Motor}(c_A + c_C) = I^*_{\rm Motor} c_{AC} \tag{5}$$

$$i^*_{BD} = I^*_{\rm Motor}(c_B + c_D) = I^*_{\rm Motor} c_{BD}. \tag{6}$$

Two switching signals s_{AC} and s_{BD} are obtained from the comparisons of two control signals and the triangular signal $v_{\rm tri}$ varying from 1 to 0. From the comparison signals and the commutation signals, all gate signals are generated by

$$G^-_X = c_X \quad X \in \{A, B, C, D\} \tag{7}$$

$$G^+_X = s_{AC} \cdot c_X \quad X \in \{A, C\} \tag{8}$$

$$G^+_X = s_{BD} \cdot c_X \quad X \in \{B, D\}. \tag{9}$$

B. Integrated Charging/Discharging Control

As SRM is at a standstill, the same four-leg asymmetrical half-bridge converter can be used to yield power from the single-phase voltage source v_s in Fig. 3.

It is noted that the frond-end bidirectional dc/dc converter with battery input still works independently to regulate the dc-link voltage V_d in charging/discharging operation. When some energy is transferred from the grid to the dc-link voltage, the transferred energy would finally charge the battery. When some energy is removed from the dc-link voltage, the equal energy may be supplied from the battery.

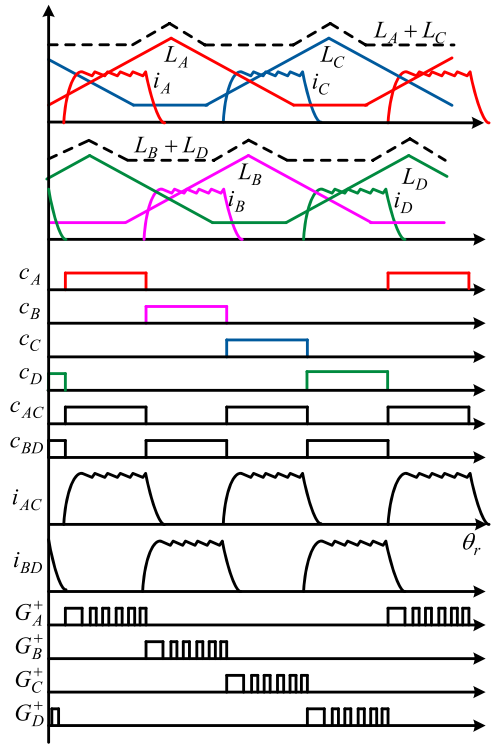

Fig. 2. Illustrated waveforms for motor driving operation.

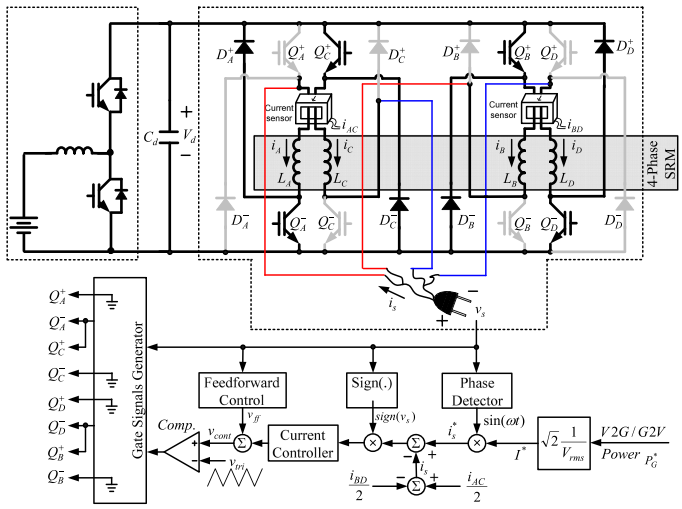

Fig. 3. Integrated four-phase SRM drive and its charging/discharging control.

In Fig. 3, the plug-in action connects the inductors in pairs, and the equivalent circuit under charging/discharging is plotted in Fig. 4 where four switches Q^+_A, Q^-_B, Q^-_C, and Q^+_D always block.

During the half-cycle of positive input voltage $v_s \geq 0$, the positive input current $i_s \geq 0$ flows though the inductances L_A and L_C, and only switches Q^-_A and Q^+_C conduct together. Therefore, the sensed current $i_{AC} = 2i_s$ is double the input current and the other sensed current is zero, $i_{BD} = 0$.

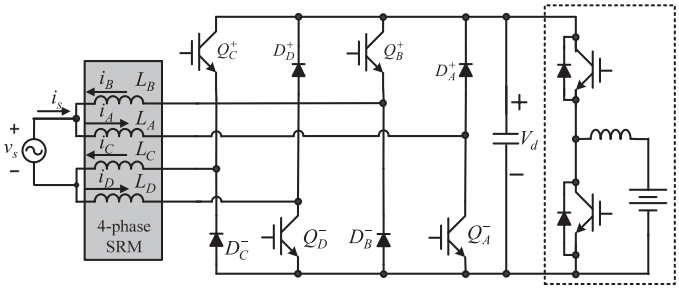

Fig. 4. Equivalent circuit under charging/discharging operation.

During the negative half-cycle $v_s < 0$, the negative input current $i_s < 0$ flows though the inductances L_B and L_D, and only switches Q_B^+ and Q_D^- conduct together. Thus, the sensed current is zero, $i_{AC} = 0$, and the other sensed current $i_{BD} = -2i_s$ is double the input current.

From Fig. 2 and (1) and (2), the total inductance $L_A + L_C$ of the flowing path during the positive half-cycle is near constant equal to the total inductance $L_B + L_D$ during the negative half-cycle. Thus, the total inductance can be seen as the constant when SRM rotor blocks at any rotor position.

Consequently, the input current i_s can be feedbacked by two physical current sensors

$$i_s = \frac{i_{AC}}{2} - \frac{i_{BD}}{2}. \tag{10}$$

From Fig. 3, the input current amplitude I^* is calculated by the desired charging/discharging power command P_G^*

$$I^* = \sqrt{2}\frac{P_G^*}{V_{\rm rms}} \tag{11}$$

where $V_{\rm rms}$ is the root-mean-square (rms) value of the input voltage v_s.

Then, the current command i_s^* is generated by multiplying the current amplitude I^* and the phase function $\sin(\omega t)$ of the input voltage v_s. According to the input voltage v_s, the current error $(i_s^* - i_s)$ is modified by multiplying the sign function $\text{sign}(v_s)$, where

$$\text{sign}(v_s) = \begin{cases} +1, & \text{when } v_s \geq 0 \\ -1, & \text{when } v_s < 0. \end{cases} \tag{12}$$

To yield the current i_s close to the current command i_s^*, the feedforward term $v_{\rm ff}$ is added to help synthesizing the control signal $v_{\rm cont}$

$$v_{\rm ff} = \frac{1}{2} - \frac{|v_s|}{2V_d}. \tag{13}$$

Under the charging/discharging operation, the gate signals are generated based on Table I. From Fig. 4, each switch is connected with a diode, no dead time is required in the gate signals.

III. Experimental Results

To evaluate the proposed integrated SRM drive, the circuit is set up and the proposed control methods are implemented in field-programmable gate array chip, as shown in Fig. 5. An 8/6 four-phase SRM is used and some parameters are tabulated in Table II. A permanent magnet synchronous motor (PMSM) is coupled to SRM to serve as the generator, and some resistor banks are connected to the PMSM windings to function as the load.

TABLE I
Gate Signal Generator

		Q_A^-	Q_B^+	Q_C^+	Q_D^-
$v_s \geq 0$	$v_{cont} \geq v_{tri}$	ON	OFF	ON	OFF
	$v_{cont} < v_{tri}$	OFF	OFF	OFF	OFF
$v_s < 0$	$v_{cont} \geq v_{tri}$	OFF	ON	OFF	ON
	$v_{cont} < v_{tri}$	OFF	OFF	OFF	OFF

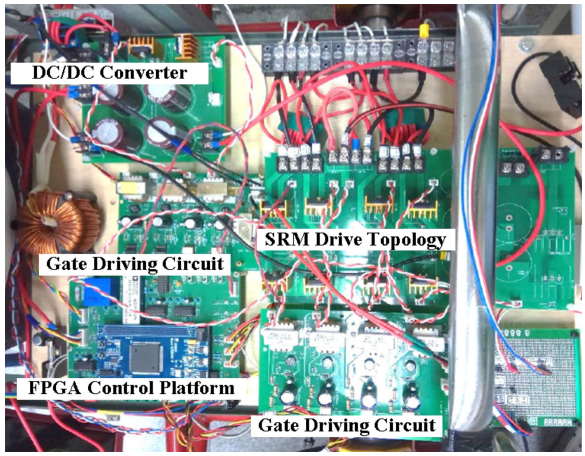

Fig. 5. Photograph of the proposed four-phase SRM drive with integrated charging/discharging function.

TABLE II
Circuit Parameters

DC-link voltage	180 V
Triangular frequency	20 kHz
DC-link capacitor	1560 uF
Input voltage value	110 Vrms
8/6 SRM winding resistance	0.45 Ω
8/6 SRM winding inductance	0.7 mH~3.63 mH

A. Motor Driving Control

The experimental steady-state waveforms at 1000 and 2000 r/min are plotted in Fig. 6(a) and (b), respectively. The gate signal G_A^- is the same as the commutation signal c_A and the gate signal G_C^- is the same as the commutation signal c_C. From Fig. 6, the yielded current i_{AC} tracks close to the synthesized current command i_{AC}^*, and the motor winding currents i_A and i_C are yielded independently.

The experimental transient waveforms due to the change of the speed command from 1000 to 1100 r/min are plotted in Fig. 7(a). The responses due to the change of the speed command from 2000 to 2100 r/min are plotted in Fig. 7(b). Because of the fixed resistor bank connected to PMSM, the current amplitude $I_{\rm Motor}^*$ increases from 9.3 to 9.8 A in Fig. 7(a) to meet the increase of SRM speed. At the same time, there is a sudden

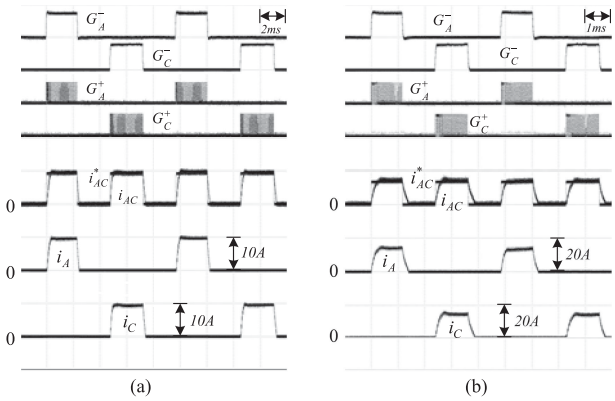

Fig. 6. Experimental steady-state waveforms at (a) 1000 r/min and (b) 2000 r/min.

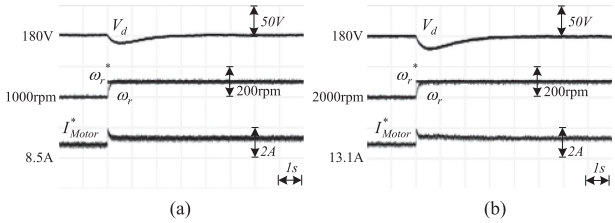

Fig. 7. Experimental transient waveforms due to the change of speed command. (a) From 1000 to 1100 r/min. (b) From 2000 to 2100 r/min.

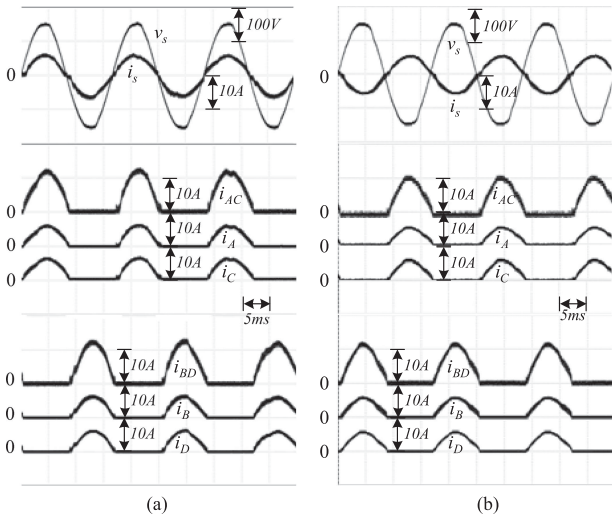

Fig. 8. Experimental waveforms during (a) charging condition and (b) discharging condition.

voltage dip in the dc-link voltage and then, some battery energy is delivered to restore the dc-link voltage.

In Fig. 7(b), the current amplitude $I^*_{\rm Motor}$ increases from 14.0 to 14.4 A and the sudden voltage dip is 20 V during the speed increase from 2000 to 2100 r/min.

From Figs. 6 and 7, the proposed SRM drive with only two current sensors is able to drive the SRM stably.

B. Integrated Charging/Discharging Control

When the SRM is at standstill, the same drive topology can be directly connected to the grid, as plotted in Fig. 3. The SRM drive equivalently works as a bidirectional ac/dc converter to transfer energy between the grid and the dc-link voltage. The experimental waveforms during charging and discharging conditions are plotted in Fig. 8(a) and (b), respectively.

In Fig. 8(a), the power command is $P_G^* = 470$ W, and the battery is charged in steady state. In addition, the battery is discharged with $P_G^* = -470$ W in Fig. 8(b). It can be found that the positive input current $i_s \geq 0$ flows through the winding inductances L_A and L_C, and one current sensor is able to sense the positive input current.

In addition, the negative input current $i_s < 0$ flows through the winding inductances L_B and L_D, and the other current sensor is able to sense the negative input current $i_{BD} = -2i_s$.

From Fig. 8, the proposed integrated SRM drive with only two current sensors is able to operate charging/discharging functions stably.

IV. Conclusion

In this letter, the integrated four-phase SRM drive with driving/charging/discharging operation is proposed and only two current sensors are required. The experimental results show that the proposed integrated SRM drive is able to provide SRM driving operation and charging/discharging operation without adding extra circuit component, current sensor, and mode selection. The proposed integrated drive can be used in SRM-based EV to provide grid-to-vehicle and vehicle-to-grid functions.

References

[1] T. J. E. Miller, *Switched Reluctance Motors and Their Control*. Oxford, U.K.: Clarendon, 1993.

[2] H. C. Chang and C. M. Liaw, "Development of a compact switched-reluctance motor drive for EV propulsion with voltage-boosting and PFC charging capabilities," *IEEE Trans. Veh. Technol.*, vol. 58, no. 7, pp. 3198–3215, Sep. 2009.

[3] Y. Hu, X. Song, W. Cao, and B. Ji, "New SR drive with integrated charging capacity for plug-in hybrid electric vehicles (PHEVs)," *IEEE Trans. Ind. Electron.*, vol. 61, no. 10, pp. 5722–5731, Oct. 2014.

[4] Y. Hu, C. Gan, W. Cao, C. Li, and S. Finney, "Split converter-fed SRM drive for flexible charging in EV/HEV applications," *IEEE Trans. Ind. Electron.*, vol. 62, no. 10, pp. 6085–6095, Apr. 2015.

[5] C. Gan, J. Wu, Y. Hu, S. Yang, W. Cao, and J. M. Guerrero, "New integrated multilevel converter for switched reluctance motor drives in plug-in hybrid electric vehicles with flexible energy conversion," *IEEE Trans. Power Electron.*, vol. 32, no. 5, pp. 3754–3766, May 2017.

[6] C. Gan, N. Jin, Q. Sun, W. Kong, Y. Hu, and L. M. Tolbert, "Multiport bidirectional SRM drives for solar-assisted hybrid electric bus powertrain with flexible driving and self-charging functions," *IEEE Trans. Power Electron.*, vol. 33, no. 10, pp. 8231–8245, Oct. 2017.

[7] H. C. Chang and C. M. Liaw, "On the front-end converter and its control for a battery powered switched-reluctance motor drive," *IEEE Trans. Power Electron.*, vol. 23, no. 4, pp. 2143–2156, Jul. 2008.

[8] H. C. Chang and C. M. Liaw, "An integrated driving/charging switched reluctance motor drive using three-phase power module," *IEEE Trans. Ind. Electron.*, vol. 58, no. 5, pp. 1763–1775, May 2011.

[9] K. T. Weng and C. Pollock, "Low-cost battery-powered switched reluctance drives with integral battery-charging capability," *IEEE Trans. Ind. Appl.*, vol. 36, no. 6, pp. 1676–1681, Nov./Dec. 2000.

[10] Z. Wang and S. Wang, "Grid power peak shaving and valley filling using vehicle-to-grid systems," *IEEE Trans. Power Del.*, vol. 28, no. 3, pp. 1822–1829, Jul. 2013.

[11] K. W. Hu, P. H. Yi, and C. M. Liaw, "An EV SRM drive powered by battery/supercapacitor with G2V and V2H/V2G capabilities," *IEEE Trans. Ind. Electron.*, vol. 62, no. 8, pp. 4714–4727, Aug. 2015.